Nano Research

ISSN 1998-0124 CN 11-5974/O4
https://doi.org/10.1007/s12274-022-4325-3

Research Article

Single-wavelength-excited fluorogenic nanoprobe for accurate real-time ratiometric analysis of broad pH fluctuations in mitophagy

Xin Zhang[1], Juan Chen[2], Jiwen Hu[1], Anna du Rietz[1], Xiongyu Wu[1], Ruilong Zhang[2] (✉), Zhongping Zhang[2], Kajsa Uvdal[1], and Zhangjun Hu[1] (✉)

[1] *Department of Physics, Chemistry, and Biology (IFM), Linköping University, Linköping SE 58183, Sweden*
[2] *School of Chemistry and Chemical Engineering, Anhui University, Hefei 230601, China*

Received: 9 December 2021 / **Revised:** 12 March 2022 / **Accepted:** 14 March 2022

ABSTRACT

Mitophagy has a critical role in maintaining cellular homeostasis through acidic lysosomes engulfing excess or impaired mitochondria, thereby pH fluctuation is one of the most significant indicators for tracking mitophagy. Then such precise pH tracking demands the fluorogenic probe that has tailored contemporaneous features, including mitochondrial-specificity, excellent biocompatibility, wide pH-sensitive range of 8.0–4.0, and especially quantitative ability. However, available molecular probes cannot simultaneously meet all the requirements since it is extremely difficult to integrate multiple functionalities into a single molecule. To fully address this issue, we herein integrate two fluorogenic pH sensitive units, a mitochondria-specific block, cell-penetrating facilitator, and biocompatible segments into an elegant silica nano scaffold, which greatly ensures the applicability for real-time tracking of pH fluctuations in mitophagy. Most significantly, at a single wavelength excitation, the integrated pH-sensitive units have spectra-distinguishable fluorescence towards alkaline and acidic pH in a broad range that covers mitochondrial and lysosomal pH, thus enabling a ratiometric analysis of pH variations during the whole mitophagy. This work also provides constructive insights into the fabrication of advanced fluorescent nanoprobes for diverse biomedical applications.

KEYWORDS

mitochondrial pH, mitophagy, ratiometric fluorescence, nanoprobe, cell imaging

1 Introduction

Mitochondria are essential organelles in cells and can be seen as the cellular powerhouses to provide energy to many biological processes [1]. Nevertheless, the mitochondria can be damaged by excess reactive oxygen species (ROS) from severe respiratory. Dysfunctional mitochondria can be eliminated by mitophagy, which is a selective form of autophagy to maintain cell homeostasis under stressful conditions [2]. If not removed, they are believed to be highly correlated with neurological [3] and cardiovascular diseases [4], and even some types of cancer [5]. Therefore, the study of mitophagy is becoming very critical to tackle mitochondrial-associated diseases by providing more and deeper understanding of molecular mechanisms and pathways.

Fluorescence microscopy (FM) has been demonstrated as an indispensable tool for autophagy studies [6]. Towards studying mitophagy by FM, specific fluorescent probes that can track the dynamics of mitophagy are of course needed. It is known that during mitophagy, mitochondria (pH ~ 8.0) are first engulfed into double-membrane vesicles named phagophore, and the cargoes are further fused with the lysosome (pH ~ 5.0) to form autolysosome for degradation [7]. Owing to the fusion process of mitochondria and lysosomes, the microenvironmental pH will obviously change during the process, detecting the pH alterations under mitophagy using a mitochondria-targeted fluorescent probe is considered as one of the efficient ways of monitoring the mitophagy process [8]. However, a variety of pH-responsive fluorescent probes are mostly based on the protonation/deprotonation of a single moiety, thereby intracellular pH measurements using these probes are limited in narrow pH ranges that cannot meet the requirement for tracking of mitophagy [9]. An ideal readout should be within a broad pH range from 8.0 to 5.0 that fully covers the pH range from mitochondria to lysosomes [10].

Herein, we strategize a new proposal to further improve the detection by taking advantage of nanomaterials, e.g., elasticity on the integration and modulation of functionalities. Based on our recently-established biocompatible hybrid fluorescent nano scaffold (FNPs) [11, 12], we integrate dual pH-sensitive xanthene-based fluorophores of fluorescein (FRC) (λ_{em} ~ 520 nm, basic pH-sensitive) and rhodamine B (RDM) (λ_{em} ~ 580 nm, acidic pH-sensitive) into a single nanoparticle (NP) [13–15]. They can be easily cross-linked to the inner core of silica nanoparticles, aiming not only to extend the pH sensing range through the integration of the two fluorophores but also to increase their sensitivity by effectively eliminating external interference from species (including oxygen, ions, proteins, enzymes, etc.) through the protective shell layer. The additional importance of this combination is that the dual-channel fluorescence from two fluorophores could be excited by one excitation (at ca. 480 nm), which will greatly facilitate the imaging operations [16]. Moreover, the intensity of the two components can be readily adjusted to

Address correspondence to Ruilong Zhang, zrl@ahu.edu.cn; Zhangjun Hu, zhangjun.hu@liu.se

achieve ideal ratiometric sensing requirements. A mitochondria-anchoring motif triphenylphosphonium (TPP), and cell-penetrating cyclic disulfide (CPCDs) are surface modified onto FNPs to enable speedy internalization and specific mitochondrial accumulation. As expected, the fabricated nanoprobe is capable of tracking pH variations during the whole mitophagy process by means of ratiometric fluorescent signals (Scheme 1).

2 Experimental section

2.1 Reagents and instruments

Pluronic® F-127, triethoxy(3-isocyanatopropyl)silane, lipoamido-dPEG®$_8$-acid (containing CPCDs), 1-ethyl-3-(3-dimethly aminopropyl) carbodiimide (EDC), N-hydroxysuccinimide (NHS), (3-aminopropyl)triethoxysilane (APTES), fetal bovine serum (FBS), phosphate-buffered saline (PBS) tablet, 3-methyladenine (3-MA), trypsin/EDTA solution, Dulbecco's modified Eagle's media (DMEM), carbonyl cyanide *m*-chlorophenyl hydrazone (CCCP), (3-carboxypropyl) triphenylphosphonium bromide (containing TPP), and diethoxydimethylsilane (DMDES) were obtained from Sigma-Aldrich. Two commercial trackers, LysoTracker Deep Red (LDR) and MitoTracker Deep Red (MDR) were obtained from ThermoFisher.

Electrospray ionization mass spectra (ESI-MS) were acquired on a Waters SQ Detector. Proton nuclear magnetic resonance (^{1}H NMR, ^{13}C NMR) measurement was performed on a Varian 500 MHz spectrometer. Transmission electron microscopes (TEM) images were obtained by a JEOL JEM-1400 Flash transmission electron microscope. Fluorescent emission spectra were conducted on a fluoromax-4 spectrophotometer. Absorption spectra were measured on a UV-2450 spectrophotometer. Zeta potential experiments and dynamic light scattering (DLS) measurements were conducted on a Malvern Zetasizer Nano ZS90 size analyzer. Confocal fluorescent images were performed on inverted Zeiss LSM800. The 3-(4,5-dimethylthiazol-2-yl)-2,5-diphenyl tetrazolium bromide (MTT) analyses were studied on TECAN infinite M1000 Pro.

2.2 Synthesis of RDM-TEOS

RDM-TEOS was synthesized according to our previous work [12].

2.3 Synthesis of FRC-TEOS

FRC-NH_2 was synthesized following the reported Ref. [17]. Into the solution of 97 mg of FRC-NH_2 (0.26 mmol) in 20 mL dry tetrahydrofuran (THF), 80 mg of 3-(triethoxysilyl) propyl isocyanate (0.32 mmol) was slowly dropped under ice water bath. The reaction is completed in 30 min. The pure product of FRC-TEOS was subsequently obtained through silica gel chromatography (ethyl acetate/dichloromethane (v/v, 20/1)). 76 mg solid of FRC-TEOS was obtained (yield, 47%). ^{1}H NMR (500 MHz, acetone-d_6): 9.08 (s, 1H), 7.85 (s, 1H), 7.56 (s, 2H), 7.07 (s, 1H), 6.70 (s, 2H), 6.54 (s, 3H), 5.60 (t, J = 16.6, 2H), 3.79 (s, 6H), 3.25 (s, 2H), 3.06 (s, 2H), 2.94 (s, 3H), 1.54 (s, 2H), 1.16 (s, 9H), and 0.57 (s, 2H). ^{13}C NMR (125 MHz, acetone-d_6): 168.06, 158.78, 153.83, 152.67, 132.73, 130.69, 128.90, 128.42, 123.71, 122.51, 112.41, 110.08, 102.63, 64.43, 57.88, 42.65, 40.54, 38.95, 23.69, 17.81, and 7.42. MS (ESI-MS): Calcd for $C_{32}H_{39}N_3O_8Si$ [M+H$^+$]: 622.76. Found 622.93.

2.4 Synthesis of RDM-NPs and FRC-NPs

For RDM-NPs, 100 mg of F-127 and 1.5 mg of RDM-TEOS (2.0 μmol) were solubilized in 1.5 mL of dry THF to give a transparent solution. THF was firstly removed by a gentle nitrogen flow, and the residual THF was further got rid of by vacuum evaporation. The resulting mixture was redispersed in 1.5 mL of hydrochloride solution (0.85 M). After adding 160 μL of TEOS, the solution was kept stirring for the interfaced hydrolysis and condensation. Then, 70 μL DMDES was added to terminate the reactions. After 24 h reaction, the solution was filtrated by a syringe filter (0.22 μm) and purified by dialysis. The nanoparticle content of the resulting solution was calculated by lyophilization

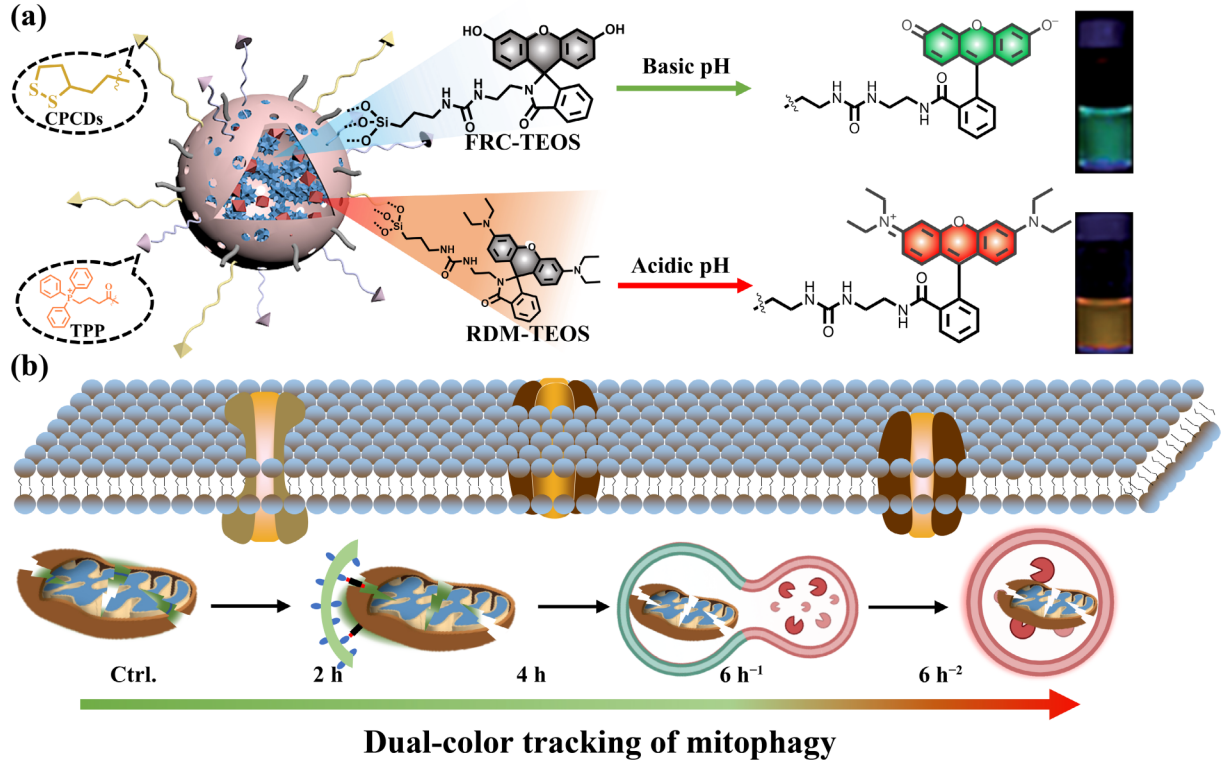

Scheme 1 Schematic illustrations: (a) structure of FR-TPP and its sensing mechanism toward pH. (b) Dual-color tracking of mitophagy.

of 0.5 mL solution. The stock solution was then made and distributed for the characterizations and other experiments. The FRC-NPs were obtained through a similar method by using 1.5 mg of FRC-TEOS (2.4 μmol).

2.5 Synthesis of FR-TPP

The synthesis of FR-TPP was similar as described above, but with different amounts of TEOS-based fluorophores (1.5 mg of FRC-TEOS, and 4.5 mg of RDM-TEOS), and APTES was used to terminate the condensation instead of DMDES and provide amino ($-NH_2$) group. NHS and EDC (70 μL, 1.0 mg·mL^{-1}) were then added to serve as coupling agents. (3-Carboxypropyl) triphenylphosphonium bromide (160 μL, 1.0 mg·mL^{-1}) was subsequently added and followed by lipoamido-dPEG®$_8$-acid (40 μL, 10 mg·mL^{-1}). The reacting solution was then stirred for 24 h. After purification, the stock solution of FR-TPP was made for the experiments. The nanoparticle content of the resulting solution was calculated by lyophilization of 0.5 mL solution.

2.6 Cytotoxicity assay

The cellular toxicity of FR-TPP was examined by the MTT assay following our previous work [12].

2.7 Cell culture and fluorescent imaging

The cells were planted on a glass-bottom micro-well dish for growth. Once the density reached the optimal, 1.0 mg·mL^{-1} of FR-TPP was added to the MCF-7 cells for 1 h of incubation. After rinsed with PBS three times and then treated with commercial MDR or LDR for another 10 min, the cells were imaged on Zeiss LSM800.

The intracellular pH titration experiments were followed by the previous work [12]. Briefly, MCF-7 cells were first incubated with FR-TPP (1.0 mg·mL^{-1}) for 1 h, then the growth medium was removed and replaced with high K^+ buffer (0.5 mM $MgSO_4$, 120 mM KCl, 30 mM NaCl, 1 mM $CaCl_2$, 1 mM NaH_2PO_4, 20 mM NaOAc, 5 mM glucose, and 20 mM HEPES) at various pH (pH = 3.0–9.0) in the presence of 10.0 μM of nigericin. The fluorescent images were obtained after 30 min of incubation.

For the mitophagy process, the cells were stimulated by CCCP (10 μM) with time after FR-TPP incubation. For mitophagy inhibition assay, the cells were stimulated by CCCP and 3-MA for 6 h. Then the fluorescent images were recorded on Zeiss LSM800.

2.8 Samples for TEM

A 5 μL drop of FR-TPP (0.2 mg·mL^{-1}) was suspended in PBS and incubated to a formvar-carbon coated copper 300 mesh electron microscopy grids (TED PELLA, Inc.). Grids were washed, blotted, and negatively stained with 2% uranyl acetate.

TEM cell images: MCF-7 cells pre-stained with FR-TTP were treated with and without CCCP, then fixed in 2.5% glutaraldehyde (Polysciences Europe GmbH, Hirschberg an der Bergstrasse, Germany) in 0.1 M phosphate buffer, pH 7.4. The fixed samples were washed in the same buffer and post fixed in 1% osmium tetroxide (Polysciences Europe GmbH, Hirschberg an der Bergstrasse, Germany). Samples were dehydrated in a series of ascending concentrations (50%, 70%, 90%, and 100%) of ethanol. A two-step infiltration in a mixture of one part absolute ethanol-one part embedding medium and 100% embedding medium was performed prior to embedding (48 h at 60 °C) in Durcupan ACM epoxy resin (Electron Microscopy Sciences, P.O. Box 550, 1560 Industry Road, Hatfield, PA 19440). The blocks were initially trimmed and sectioned using a Leica UC7 ultramicrotome (Leica Microsystems GmbH, Vienna, Austria). Ultrathin sections (60-nm thickness) were collected onto a formvar-coated copper slot grid, and counter stained with uranyl acetate and lead citrate. Images were taken using an 80 kV transmission electron microscope (JEOL JEM1400 Flash, JEOL Ltd., Tokyo, Japan).

3 Results and discussion

3.1 Design and synthesis of pH-responsive nanoprobes

The structures of RDM-TEOS and FRC-TEOS were confirmed by ^{1}H NMR, ^{13}C NMR, and ESI-MS spectroscopy measurements (Scheme S1 and Figs. S1–S3 in the Electronic Supplementary Material (ESM)). To study pH sensitivity of the tailored fluorophores, RDM-TEOS and FRC-TEOS are employed to generate RDM-NPs and FRC-NPs, respectively (Fig. 1 and Scheme S2 in the ESM) [12]. The emission spectra of the two nanoprobes in buffer solutions with various pH values are measured (Figs. 1(b) and 1(d)). With the increase of pH, the emission intensity at 520 nm from FRC-NPs gradually enhances, and the fluorescence at 580 nm from RDM-NPs regularly decreases. The calibration plots reveal quite narrow sensitive pH ranges that occur between pH 6.0–8.5 for FRC-NPs (pK_a, 6.95), and pH 4.5–5.5 for RDM-NPs (pK_a, 5.64), respectively (Fig. S4 in the ESM and Table 1). Obviously, neither of them alone is suitable for monitoring the whole process of mitophagy starting from mitochondria (pH ~ 8.0) and ending up in lysosomes (pH ~ 5.0). However, based on these results, it can be anticipated that the integration of RDM and FRC with an appropriate ratio into a single nanoparticle may fulfill such demand. Therefore, to verify our hypothesis, initially, we fabricated such nanoparticles with a mass ratio of 1:1 (RDM-TEOS:FRC-TEOS). As shown in Fig. S5 in the ESM, the increasing pH induces higher fluorescence intensity at 520 nm while the intensity at 580 nm shows slight increases, but no such significant difference. We reason that at this condition, the fluorescence intensity from FRC-TEOS is much higher than that from RDM-TEOS under the same excitation, which results in this phenomenon. However, this result then can give us clear guidance for adjusting the proportions of the incorporated FRC-TEOS and RDM-TEOS to reach comparable pH-induced intensity changes of the emission bands at 520 and 580 nm (Fig. 2(a)) [12]. Briefly, we fixed the content of FRC-TEOS (1.5 mg) in NPs which can give us relatively high fluorescence intensity, then we adjusted the contents of RDM-TEOS unit to reach a comparable fluorescence at pH 3. Ultimately, the proportion of FRC and RDM in a single nanoparticle is optimized and finalized as 1:3 (the mass ratio of FRC-TEOS:RDM-TEOS). To further endow the nanoparticles with mitochondrial specificity and efficient cellular uptake, TPP and CPCDs are then grafted onto the surface to give final FR-TPP (Fig. S6 in the ESM) [11, 12].

The fluorescence sensing behaviors of FR-TPP toward pH values are subsequently studied. As shown in Fig. 2(b), with increasing pH values from 3.0–10.0, the emission at 520 nm (green emission) raises gradually while emission at 580 nm (orange-red emission) descends, resulting in significant ratiometric signal changes. The ratios of dual-color fluorescence are highly related to pH changes as shown in the sigmoidal plot in Fig. 2(c). Compared to those of RDM-NPs and FRC-NPs, a wider linear range (pH 4.5–8.0) is achieved (Table 1 and Fig. S7 in the ESM). In addition, no signal attenuation can be observed when repeatedly switching between pH 4.0 and 7.0, suggesting that FR-TPP possesses remarkable reversibility to pH (Fig. S8 in the ESM). Afterward, the study on interference to the response fluorescence is conducted (Fig. S9 in the ESM). Negligible influences are observed in the presence of tested substances.

Although the photophysical studies suggest that FR-TPP is very promising for intended cellular monitoring. The morphology and the size distribution of FR-TPP are additional important

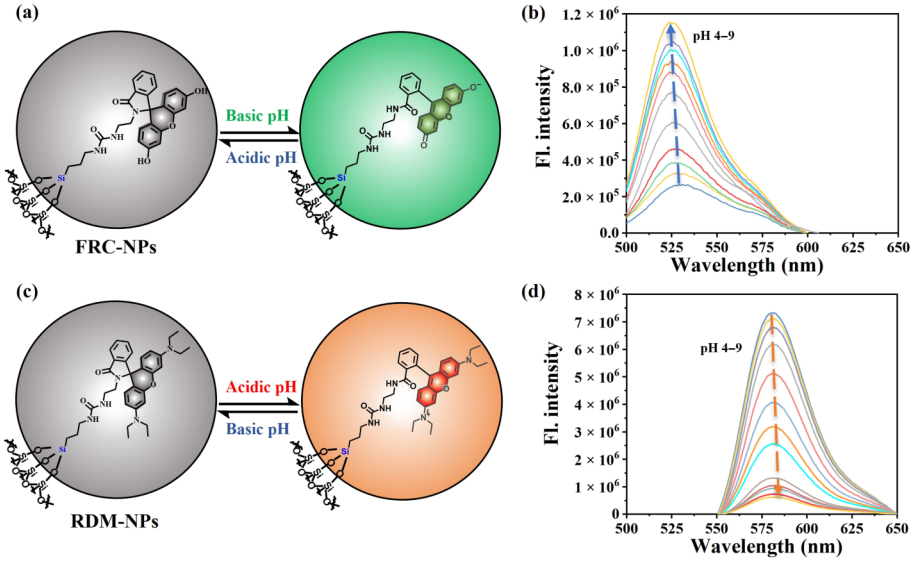

Figure 1 (a) Responsive mechanism of FRC-NPs for pH sensing. (b) Fluorescence response of FRC-NPs (1.0 mg·mL^{-1}) towards different pH under 480 nm excitation. (c) Responsive mechanism of RDM-NPs for pH sensing. (d) Fluorescence response of RDM-NPs (1.0 mg·mL^{-1}) towards different pH under 480 nm excitation.

Table 1 Summarize linear relationship among different nanoprobes

Probes	Linear range
RDM-NPs	4.5–5.5
FRC-NPs	6.0–8.5
FR-TPP	4.5–8.0

parameters for the nanomaterials used in cell studies. TEM and DLS measurements are then conducted to characterize FR-TPP. DLS result determines that the average hydrodynamic diameter of FR-TPP is around 40 nm (Fig. 2(d)). TEM image reveals that FR-TPP has a uniform and spherical shape with a core–shell structure (Fig. 2(e) and inset). Positive zeta potential of 16 ± 2.3 mV is obtained since the cation of TPP is grafted on the outer layer of NPs.

3.2 Cytotoxicity and photobleaching

Traditional MTT assay is used to study the cell viabilities at varied concentrations of FR-TPP for 24 h (Fig. S10(a) in the ESM). The cell viability with FR-TPP (2.0 mg·mL^{-1}) is above 85%, indicating that FR-TPP exhibits negligible cytotoxicity to cells. Further, photophysical stability of FR-TPP is performed. The collected fluorescent signals are comparatively stable during the constant irradiation (150 W xenon lamp) (Fig. S10(b) in the ESM). Overall, these results indicate that FR-TPP is very promising for further studies of intracellular pH-related processes.

3.3 Ratiometric cell imaging

To assess the ability of FR-TPP to monitor intracellular pH fluctuations, pH titration experiments in MCF-7 cells are carried out, where high K^+ buffer and ionophore nigericin (10 μM) are utilized to manipulate the intracellular pH values (Fig. 3(a)) [18]. It can be seen that fluorescence intensity from the green channel (510–540 nm) is gradually enhanced upon pH increasing from 3.0 to 9.0, while the intensity from the red channel (570–600 nm) generally decreases. The resulting ratios of the two channels (F_{green}/F_{red}) exhibit linearity in the pH range 4.0–8.0 (Fig. 3(b), red line, R^2 = 0.98), which basically covers the pH changes during mitophagy. These results indicate that FR-TPP can be utilized for ratiometric tracking pH value in living cells.

To verify the subcellular location of FR-TPP in living cells, co-localization imaging experiments are conducted by co-incubation of FR-TPP and a commercially mitochondria-specific dye, MitoTracker Deep Red. As shown in Fig. 3(c), the image from the green channel (from FR-TPP) shows filamentous morphology, and the fluorescence distribution merges well with the MDR channel, which results in a good R_r value (Pearson's colocalization

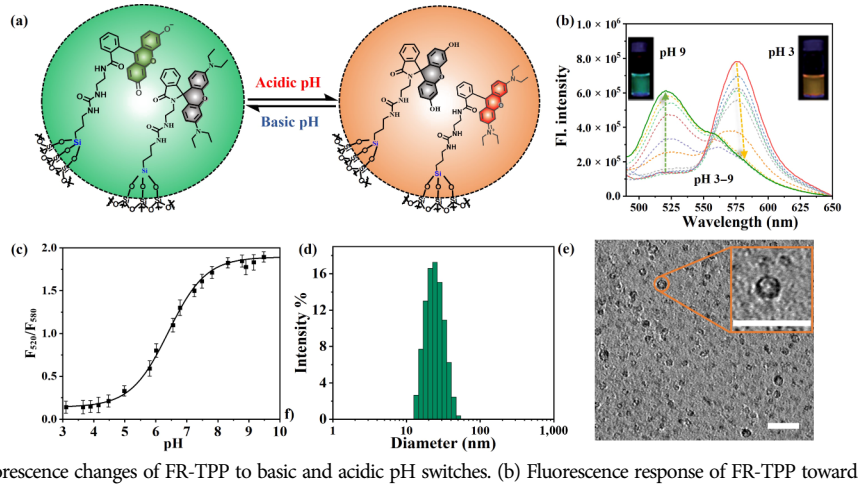

Figure 2 (a) Dual-color fluorescence changes of FR-TPP to basic and acidic pH switches. (b) Fluorescence response of FR-TPP toward different pH under 480 nm excitation. (c) The relationship between F_{520}/F_{580} and pH based on panel (b). (d) The average size distribution of FR-TPP. (e) TEM image of FR-TPP, scale bar = 50 nm.

coefficient, 0.75). Taken together, these results demonstrate that FR-TPP has the capability to selectively target mitochondria in living cells and quantitatively monitor mitochondrial pH fluctuations.

3.4 Monitoring mitochondrial pH change during mitophagy

After the above basic confirmatory experiments, FR-TPP is then used to monitor dynamic mitochondrial pH changes during mitophagy via a dual-channel mode. First, in a nutrient-rich medium, the MCF-7 cells are co-incubated with FR-TPP, LysoTracker Deep Red (a lysosomal tag), and stimulated by carbonyl cyanide *m*-chlorophenyl hydrazone (a membrane potential uncoupler that can induce mitophagy) [19]. As shown in Fig. 4(a), initially, the cells show intensive fluorescence in the green channel while no fluorescence is in the red channel, giving a low-intensity ratio (F_{red}/F_{green}) and high mitochondrial pH (Fig. 4(b)). After the stimulation with CCCP for 2 h, the red channel shows a slightly increased fluorescence while the green channel shows decreased fluorescence simultaneously. After 4 h stimulation, the fluorescence intensity in the red channel is further enhanced, while the green channel shows a persisting decrease. When the stimulation period is afterward extended to 6 h, the evident increase in the red channel and decrease in the green channel are even more clear. As noted in the dramatic increase in fluorescence ratio, this visual evidence of pH change can indicate the mitophagy process. Meanwhile, the filamentous morphologies of mitochondria are gradually disappeared in the green channel, with more bright spots appearing in the red channel after 6 h, which is consistent with the features of lysosomes. It also gives higher R_r values over time between the red and LDR channels (Fig. 4(c)), which means that autolysosomes gradually generate meanwhile resulting in persisting decrease of mitochondrial pH [8]. The pH alterations in mitochondria are able to be quantitatively calculated through the pH calibration curve (Fig. 3(b)). As a result, initially, the average pH value of mitochondria is calculated to be 7.98 ± 0.41 while the CCCP-induced mitophagy drives the pH to decrease to 7.49 ± 0.25, 7.20 ± 0.16, and 5.51 ± 0.19 with the incubation time of 2, 4, and 6 h (Fig. 4(b)), respectively.

To further verify this process, a mitophagy inhibition assay is performed with the cells that are pre-treated with 3-MA, an autophagy inhibitor for blocking autophagosome formation [20]. As shown in Fig. S11 in the ESM, the cells incubated with 3-MA and CCCP for 6 h showed no emission in the red channel compared to the cells treated only with CCCP in Fig. 4(a), and strong emission in the green channel, illustrating the process of mitophagy is inhibited. In addition, the extra control experiments are performed to exclude the possibility that long cell incubation time could also cause the generation of autolysosomes and a decrease of mitochondrial pH. As can be seen in Fig. S11 in the ESM, after 6 h of incubation, the green channel gives a strong fluorescence while fluorescence in the red channel is negligibly detected, indicating that long-term cell cultivation hardly contributes to mitophagy and pH fluctuations. Meanwhile, western blot (WB) experiments are conducted to investigate whether mitophagy occurs by monitoring the autophagy markers protein LC3 and P62 [21]. When autophagy is initiated, LC3-I will convert to LC3-II through conjugation with phosphatidylethanolamine [22]. Subsequently, the ubiquitin-

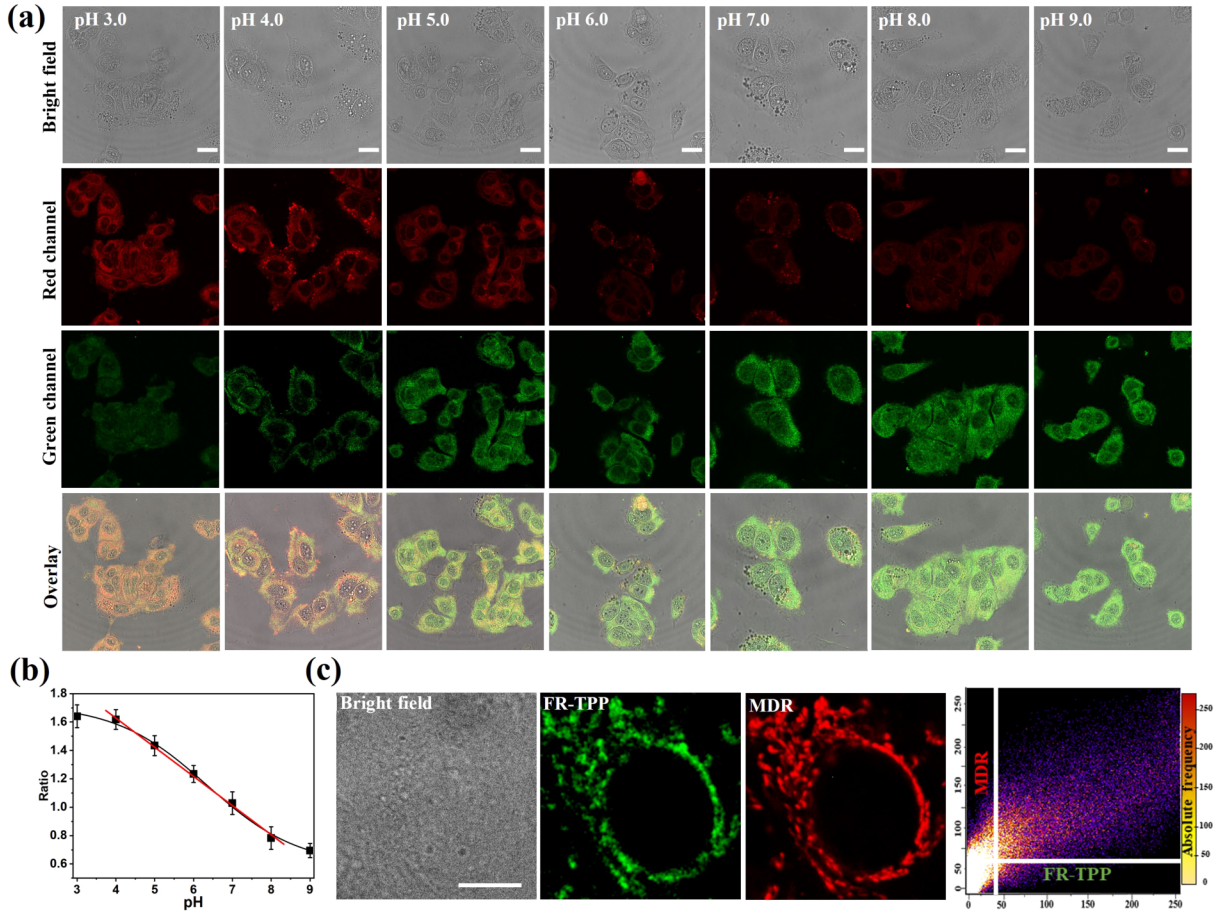

Figure 3 (a) Confocal images of MCF-7 cells with different intracellular pH stained with FR-TPP, scale bar = 10 μm. (b) The relationship between fluorescence intensity ratio of F_{red}/F_{green} and pH, the red line indicates linearity in pH range of 4.0–8.0. (c) Colocalization experiments of MCF-7 cells treated with FR-TPP for 1 h and MDR for another 10 min, scale bar = 10 μm. Green channel is collected from 510–540 nm, with an excitation at 488 nm; red channel is collected from 570–600 nm, with an excitation at 488 nm; MDR channel is collected from 658–668 nm, with an excitation at 647 nm.

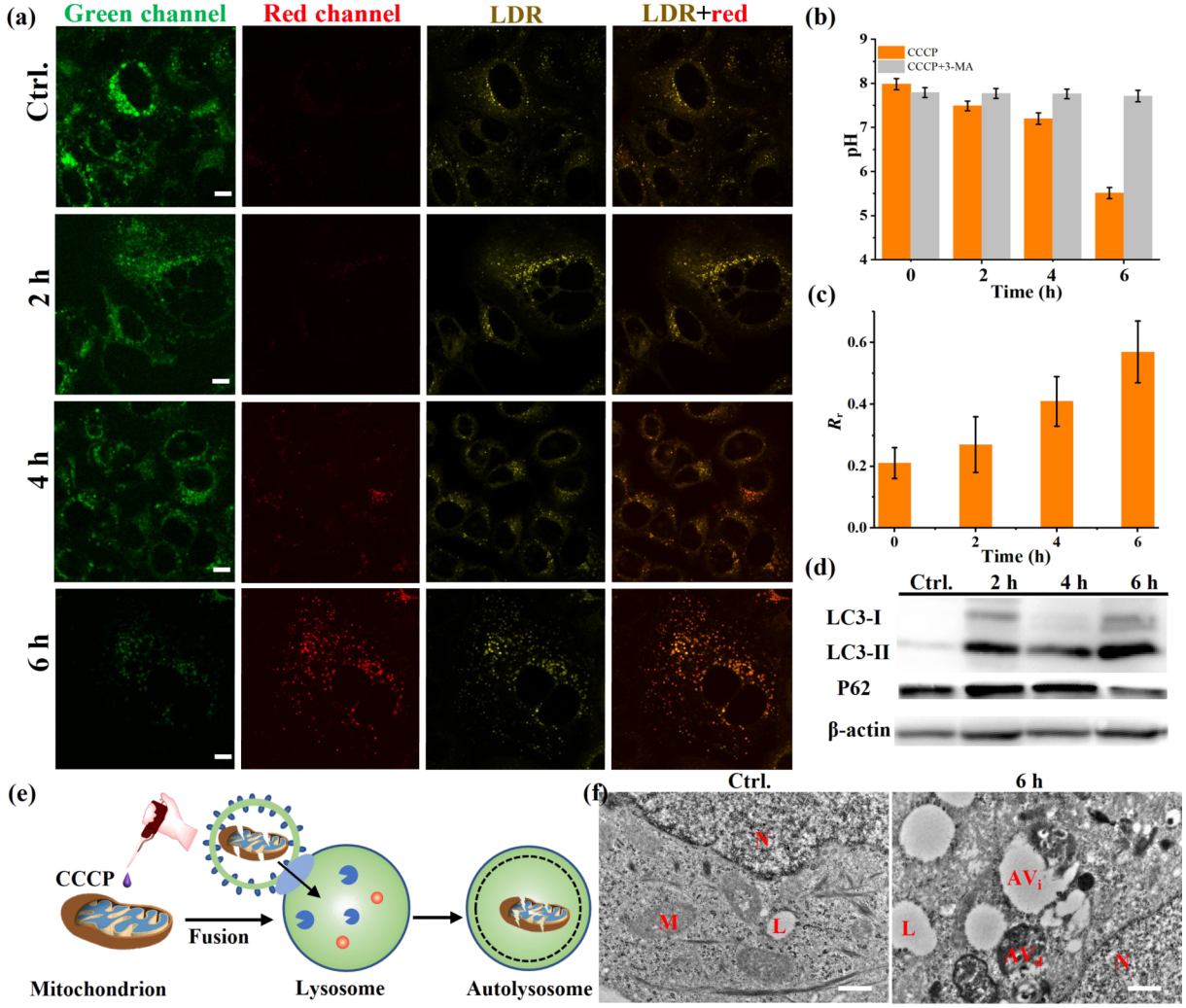

Figure 4 (a) Confocal images of MCF-7 cells treated with FR-TPP and LDR under CCCP treatment at different durations, scale bar = 10 μm. Green channel is collected from 510–540 nm, with an excitation at 488 nm; red channel is collected from 570–600 nm, with an excitation at 488 nm; and LDR channel is collected from 658–668 nm, with an excitation at 647 nm. (b) The pH changes under various treatments at various durations. (c) R_r changes between the red and LDR channels during mitophagy. (d) Western blot analysis of autophagy-associated proteins under CCCP treatment at various durations. (e) Schematic illustration of CCCP-induced mitophagy process. (f) Representative TEM images of the cytoplasmic regions of MCF-7 cells with CCCP treatment, scale bar = 500 nm. N = nucleus, L = lysosome, M = mitochondrion, AV_i = autophagosome, and AV_d = degradative autophagic vacuole.

binding protein P62 will interact with LC3-II and thereby deliver to autophagosomes for degradation [23]. As shown in Fig. 4(d), it revealed an increased intensity in LC3-II, as well as a decreased intensity in P62 with CCCP treatment over time, indicating the activation of autophagy. Eventually, TEM measurement is used to confirm the mitophagy process. As shown in Fig. 4(f), the mitochondrion and lysosome can be vividly observed in cells without CCCP treatment. However, after 6 h of incubation of CCCP, the formation of autophagosomes (AV_i) and autolysosomes (AV_d) which are filled by small internal vesicles could be observed. These results matched well with those was monitored by the utility of FR-TPP.

4 Conclusions

In summary, by incorporating two acidic sensitive and alkaline sensitive fluorophores into a single nanoparticle, we have developed FR-TPP serving as a broad pH-responsive ratiometric fluorescent nanoprobe with high mitochondrial specificity. The profits from the ratiometric and mitochondria-specific features make the tailored FR-TPP able to quantitatively track mitochondrial pH fluctuations associated with the acidifications and fusions processes during mitophagy. The results demonstrate that FR-TPP is a promising fluorescent pH nanoprobe for investigating the roles of mitochondria in different intracellular processes. In addition, the synthetic convenience of this nanoprobe can give useful guidance to the fabrication of other probes for various biological imaging and sensing purposes.

Acknowledgements

This work is supported by STINT Joint China-Sweden Mobility Project (No. CH2017-7243), the Swedish Research Council (VR) (Nos. 2019-02409 and 2020-05437), the China Scholarship Council (CSC), Carl Tryggers Stiftelse (No. CTS 19:379), Swedish Government strategic faculty grant in material science (SFO, MATLIU) in Advanced Functional Materials (AFM) (VR No. 5.1-2015-5959), the Centre in Nano Science and technology at LiTH (CeNano), and LiU Cancer network at Linköping University.

Funding note: Open access funding provided by Linköping University

Electronic Supplementary Material: Supplementary material (^{1}H NMR spectrum, ^{13}C NMR spectrum, MS spectrum, photon-physical properties, standard MTT assays, photo-stability experiments, and fluorescence cell images) are available in the online version of this article at https://doi.org/10.1007/s12274-022-

4325-3.

References

[1] Sterea, A. M. ; El Hiani, Y. The role of mitochondrial calcium signaling in the pathophysiology of cancer cells. *Adv. Exp. Med. Biol.* **2020**, *1131*, 747–770.

[2] Onishi, M.; Yamano, K.; Sato, M.; Matsuda, N.; Okamoto, K. Molecular mechanisms and physiological functions of mitophagy. *EMBO J.* **2021**, *40*, e104705.

[3] Kang, T. C. Nuclear factor-erythroid 2-related factor 2 (Nrf2) and mitochondrial dynamics/mitophagy in neurological diseases. *Antioxidants* **2020**, *9*, 617.

[4] Chistiakov, D. A.; Shkurat, T. P.; Melnichenko, A. A.; Grechko, A. V.; Orekhov, A. N. The role of mitochondrial dysfunction in cardiovascular disease: A brief review. *Ann. Med.* **2018**, *50*, 121–127.

[5] Porporato, P. E.; Filigheddu, N.; Bravo-San Pedro, J. M.; Kroemer, G.; Galluzzi, L. Mitochondrial metabolism and cancer. *Cell Res.* **2018**, *28*, 265–280.

[6] Rai, S.; Manjithaya, R. Fluorescence microscopy: A tool to study autophagy. *AIP Adv.* **2015**, *5*, 084804.

[7] Shi, R. Y.; Guberman, M.; Kirshenbaum, L. A. Mitochondrial quality control: The role of mitophagy in aging. *Trends Cardiovas. Med.* **2018**, *28*, 246–260.

[8] Li, X. Y.; Hu, Y. M.; Li, X. H.; Ma, H. M. Mitochondria-immobilized near-infrared ratiometric fluorescent pH probe to evaluate cellular mitophagy. *Anal. Chem.* **2019**, *91*, 11409–11416.

[9] Yuan, J.; Peng, R.; Cheng, D.; Zou, L. H.; Yuan, L. Revealing minor pH changes of mitochondria by a highly sensitive molecular fluorescent probe. *Chem. Asian J.* **2021**, *16*, 342–347.

[10] Wang, H.; Hu, J. W.; Yang, G. Q.; Zhang, X.; Zhang, R. L.; Uvdal, K.; Zhang, Z. P.; Wu, X. Y.; Hu, Z. J. Real-time tracking of mitochondrial dynamics by a dual-sensitive probe. *Sens. Actuators B:Chem.* **2020**, *320*, 128418.

[11] Zhang, X.; Wang, C. F.; Feng, G.; Jiang, J. X.; Hu, J. W.; du Rietz, A.; Brommesson, C.; Zhang, X. J.; Ma, Y. G.; Roberg, K. et al. Tailorable membrane-penetrating nanoplatform for highly efficient organelle-specific localization. *Small* **2021**, *17*, 2101440.

[12] Zhang, X.; du Rietz, A.; Hu, J. W.; Brommesson, C.; Wu, X. Y.; Uvdal, K.; Hu, Z. J. A ratiometric fluorogenic nanoprobe for real-time quantitative monitoring of lysosomal pH. *Sens. Actuators B:Chem.* **2021**, *345*, 130350.

[13] Lee, M. H.; Han, J. H.; Lee, J. H.; Park, N.; Kumar, R.; Kang, C.; Kim, J. S. Two-color probe to monitor a wide range of pH values in cells. *Angew. Chem.* **2013**, *125*, 6326–6329.

[14] Zheng, H.; Zhan, X. Q.; Bian, Q. N.; Zhang, X. J. Advances in modifying fluorescein and rhodamine fluorophores as fluorescent chemosensors. *Chem. Commun.* **2013**, *49*, 429–447.

[15] Le Guern, F.; Mussard, V.; Gaucher, A.; Rottman, M.; Prim, D. Fluorescein derivatives as fluorescent probes for pH monitoring along recent biological applications. *Int. J. Mol. Sci.* **2020**, *21*, 9217.

[16] Lee, M. H.; Han, J. H.; Lee, J. H.; Park, N.; Kumar, R.; Kang, C.; Kim, J. S. Two-color probe to monitor a wide range of pH values in cells. *Angew. Chem., Int. Ed.* **2013**, *52*, 6206–6209.

[17] Yu, K. K.; Li, K.; Qin, H. H.; Zhou, Q.; Qian, C. H.; Liu, Y. H.; Yu, X. Q. Construction of pH-sensitive "submarine" based on gold nanoparticles with double insurance for intracellular pH mapping, quantifying of whole cells and *in vivo* applications. *ACS Appl. Mater. Interfaces* **2016**, *8*, 22839–22848.

[18] Luo, X.; Yang, H. T.; Wang, H. L.; Ye, Z. W.; Zhou, Z. N.; Gu, L. Y.; Chen, J. Q.; Xiao, Y.; Liang, X. W.; Qian, X. H. et al. Highly sensitive hill-type small-molecule pH probe that recognizes the reversed pH gradient of cancer cells. *Anal. Chem.* **2018**, *90*, 5803–5809.

[19] Livingston, M. J.; Wang, J. H.; Zhou, J. L.; Wu, G. Y.; Ganley, I. G.; Hill, J. A.; Yin, X. M.; Dong, Z. Clearance of damaged mitochondria via mitophagy is important to the protective effect of ischemic preconditioning in kidneys. *Autophagy* **2019**, *15*, 2142–2162.

[20] Wang, X. D.; Fan, L.; Wang, S. H.; Zhang, Y. W.; Li, F.; Zan, Q.; Lu, W. J.; Shuang, S. M.; Dong, C. Real-time monitoring mitochondrial viscosity during Mitophagy using a mitochondria-immobilized near-infrared aggregation-induced emission probe. *Anal. Chem.* **2021**, *93*, 3241–3249.

[21] Ha, S.; Jeong, S. H.; Yi, K.; Chung, K. M.; Hong, C. J.; Kim, S. W.; Kim, E. K.; Yu, S. W. Phosphorylation of p62 by AMP-activated protein kinase mediates autophagic cell death in adult hippocampal neural stem cells. *J. Biol. Chem.* **2017**, *292*, 13795–13808.

[22] Bansal, M.; Moharir, S. C.; Swarup, G. Autophagy receptor optineurin promotes autophagosome formation by potentiating LC3-II production and phagophore maturation. *Commun. Integr. Biol.* **2018**, *11*, 1–4.

[23] Li, Q. R.; Han, Y.; Du, J. B.; Jin, H. F.; Zhang, J.; Niu, M. M.; Qin, J. Alterations of apoptosis and autophagy in developing brain of rats with epilepsy: Changes in LC3, P62, Beclin-1 and Bcl-2 levels. *Neurosci. Res.* **2018**, *130*, 47–55.